Atmos. Chem. Phys. Discuss., 5, 8649–8688, 2005
www.atmos-chem-phys.org/acpd/5/8649/
SRef-ID: 1680-7375/acpd/2005-5-8649
European Geosciences Union

Atmospheric Chemistry and Physics Discussions

Measurements of NO, NO_y, N_2O, and O_3 during SPURT: implications for transport and chemistry in the lowermost stratosphere

M. I. Hegglin[1,*], D. Brunner[1], Th. Peter[1], P. Hoor[2], H. Fischer[2], J. Staehelin[1], M. Krebsbach[3], C. Schiller[3], U. Parchatka[2], and U. Weers[1]

[1]Institute for Atmospheric and Climate Science, Swiss Federal Institute of Technology, Zurich, Switzerland
[2]Max Planck Institute for Chemistry, Air Chemistry, Mainz, Germany
[3]Institute for Chemistry and Dynamics of the Geosphere: Stratosphere, Research Centre Jülich GmbH, Jülich, Germany
[*]now at: Atmospheric Physics, University of Toronto, 60 St. George Street, Toronto, Ontario, M5S 1A7, Canada

Received: 22 August 2005 – Accepted: 1 September 2005 – Published: 13 September 2005

Correspondence to: M. I. Hegglin (michaela@atmosp.physics.utoronto.ca)

Abstract

We present measurements of NO, NO_y, O_3, and N_2O within the lowermost stratosphere (LMS) over Europe obtained during the SPURT project. The measurements cover each of the four seasons during two years between November 2001 and July 2003, and probe the entire altitude and latitude range of the LMS: from 5° N to 85° N equivalent latitude, and from 290 to 375 K potential temperature. The measurements represent a comprehensive data set of these tracers and reveal atmospheric transport processes that influence tracer distributions in the LMS. Mean mixing ratios of stratospheric tracers in equivalent latitude-potential temperature coordinates show a clear seasonal cycle related to the Brewer-Dobson circulation with highest values in spring and lowest values in autumn. Vertical profiles show strong gradients at the extratropical tropopause suggesting that vertical (cross-isentropic) mixing is reduced above the tropopause. Mixing along isentropes is also strongly reduced since pronounced meridional gradients are found on potential temperature surfaces in the LMS. Concurrent large gradients in PV in the vertical and in the meridional direction horizontally suggest the presence of a transport and mixing barrier. Well above the tropopause distinguished seasonal cycles were found in the correlation slopes $\Delta O_3/\Delta N_2O$ and $\Delta NO_y/\Delta N_2O$. Smallest slopes found during spring indicate chemically aged stratospheric air originating from high altitudes and latitudes. The slopes are larger in summer and autumn suggesting that a substantial fraction of air takes a 'short-cut' from the tropical tropopause region into the extratropical LMS. The comparison of measured NO with critical NO values at which net ozone production changes from negative to positive implies a net ozone production up to 20 K above the local tropopause in winter, increasing during spring and summer to up to 50 K in autumn. Above this height NO values favor ozone destruction.

1. Introduction

Knowledge of the chemical composition of the upper troposphere/lowermost stratosphere (UT/LMS) and of its possible trends is needed to understand feedback mechanisms between dynamics, transport, radiation, and chemistry in a changing climate. Changes in O_3 distributions lead to direct radiative forcing with strong influence on surface temperatures (Lacis et al., 1990; Forster and Shine, 1997).

Reactive nitrogen (NO_y, i.e. the sum of all species with nitrogen in oxidation states higher than +1) plays a key role in ozone chemistry involving gas-phase and heterogeneous reactions. In the stratosphere above about 18 km NO_x (=NO+NO_2) lead to net ozone destruction in catalytic cycles, whereas in the troposphere and LMS NO_x tend to act together with hydrocarbons and carbon monoxide as important precursors of ozone formation (IPCC, 1999). The UT/LMS represents a complex chemical regime with respect to temperature, pressure and chemical composition, but up to now relatively few measurements are available. Existing climatologies of NO_y, NO_x, and other atmospheric key species involved in ozone chemistry which were derived from satellite measurements and passenger aircraft either lack resolution and accuracy in the tropopause region or are limited with respect to altitude. A compilation of 30 aircraft campaigns between 1983 and 1996 yielding a tropospheric climatology has been provided by Emmons (2000). More recent measurements were presented by Kondo et al. (1997), Singh et al. (1997), Ziereis et al. (2000), and Baehr et al. (2003). The first long-term observations of NO_x and O_3 in the UT/LMS of the Northern hemisphere were made during the Swiss NOXAR project and the European POLINAT-2 project using a commercial aircraft as measurement platform (Brunner et al., 2001). O_3 and NO_y are being measured by MOZAIC since 1994 and 2001, respectively (Volz-Thomas et al., 2005). Strahan et al. (1999a, b) presented a climatology of stratospheric NO_y, O_3, and N_2O measurements defining the upper boundary to the lowermost stratosphere (LMS) region at ER-2 flight levels showing the influence of atmospheric transport processes on the distributions of long-lived trace gas species.

ACPD
5, 8649–8688, 2005

NO_y in the stratosphere is mainly produced by oxidation of N_2O but may have other sources in the LMS such as lightning, aircraft emission or deep convective injection of polluted planetary boundary layer air (Hegglin et al., 2004, and references therein). In general, tracer distributions in the LMS are therefore influenced by both, the global mean meridional circulation (or Brewer-Dobson circulation), and stratosphere-troposphere exchange (STE) processes through the extratropical tropopause (Holton et al., 1995). Climatological studies of STE events for instance by using Lagrangian model approaches yield improved quantitative information about their seasonality and spatial distribution (Wernli and Bourqui, 2002; Sprenger and Wernli, 2003; James et al., 2003). However, to get more information to which degree STE leads to irreversible mixing and how it influences the vertical and latitudinal distribution of trace gas species extensive trace gas measurements are needed. The SPURT CO measurements presented by Hoor et al. (2004) reveal the existence of a mixing layer within the first 20 to 30 K above the local tropopause during all seasons showing a strong tropospheric influence. However, STE may differently influence the distributions of trace gas species with different source/sink characteristics or microphysical behavior. A tropospheric tracer which is well-mixed in the troposphere such as N_2O or CO may show less variability compared to one with localized sources and sinks (e.g. NO_y, H_2O).

Here we present high resolution and high sensitivity airborne data of NO, NO_y, N_2O, and O_3 obtained during eight seasonally conducted measurement campaigns focusing on the LMS region up to 13.7 km within the SPURT (German: SPURenstofftransport in der Tropopausenregion) project. The data reveal new information about the seasonal distribution of the measured trace gas species and represent a valuable contribution to the existing climatology filling partly the gap between the tropopause and the 380 K isentrope. The key species involved in ozone chemistry measured during SPURT further allow a first characterization of the chemical regime prevailing in the LMS. This paper is part of the SPURT special issue in ACP where other tracer data together with tracer-specific evaluations are presented. An overview of the SPURT project is provided by Engel et al. (2005).

ACPD
5, 8649–8688, 2005

A short description of the used measurement systems, their performance and overall accuracies is given in Sect. 2. Section 3 describes the applied evaluation methods, the equivalent latitude-potential temperature coordinate mapping, the vertical profiles in $\Delta\Theta$ from the tropopause, and the tracer-tracer correlation concept. Section 4.1 presents mean tracer distributions which are suited as diagnostics for the validation of chemical transport models (CTMs) and global circulation models (GCMs) in particular concerning transport processes such as the mean meridional circulation or STE. Section 4.2 discusses the vertical profiles of median tracer values with focus on seasonality in the UT/LMS. Section 4.3 shows analyses of tracer-tracer correlations yielding information about the air mass origin in different seasons. Section 4.4 finally defines the chemical regime expected to prevail in the LMS based on the measured NO, CO (Hoor et al., 2004), and O_3 mixing ratios.

2. Chemical measurements

During SPURT a total of 36 flights were performed, each providing data from 3 to 5 flight hours. The flights covered a latitudinal range between 30° N and 75° N. A Learjet 35A reaching flight altitudes of up to 13.7 km has been used as measurement platform.

NO_y, NO, and O_3 were measured using a three channel chemiluminescence detector ECO-Physics CLD 790-SR for fast and highly sensitive measurements, in the following termed 'ECO'. The measurement principle is based on chemiluminescence obtained in the reaction between NO and O_3 yielding NO_2 in an electronically excited state (Fontijn et al., 1970). Relaxation occurs through quenching and partly through emission of light. If one reactant is supplied in excess, then the light intensity is proportional to the volume mixing ratio of the other reactant. Following this principle, NO is measured by adding an excess of O_3, while O_3 is measured by using an excess of NO as reactant.

Total reactive nitrogen (NO_y=NO + NO_2 + NO_3 + HNO_3 + HNO_4 + HONO + PAN + $RONO_2$ + $ClONO_2$ + 2×N_2O_5 + $BrONO_2$ + organic nitrate + particulate nitrate (<1 μm)) was measured by chemiluminescence after reducing NO_y species to NO by

ACPD
5, 8649–8688, 2005

means of an externally mounted catalytic gold converter with CO as reduction agent (Fahey et al., 1985). The converter samples in backward direction in order to exclude particles with diameter >1 µm. For technical details of the converter see Lange et al. (2002).

The conversion efficiency of the analyzer was quantified by using gas phase titration (GPT) of NO with O_3 to produce NO_2 before and after each campaign. With the exception of the first campaign (Hegglin et al., 2004), the conversion efficiency did not significantly change over the 7 days of a campaign and varied between 95% and 98%. The sensitivities of the NO and NO_y channels were calibrated twice during the flight by adding known amounts of NO (Sauerstoffwerk Lenzburg AG: 9.4 ppm±2% NO in N_2) showing that its sensitivity varied by less than 3.5%. The chemiluminescence detector was switched every 2 min for 10 s to pre-chamber mode in order to determine the instrument background signal (Ridley and Howlett, 1974). In addition, zero calibrations with synthetic air were performed three times during each flight to determine the temporal evolution of the NO_y artifact signal which is a common feature in NO_y measurements. Its origin is not fully understood but is in part due to impurities of the CO reduction agent (Fahey et al., 1985). Note that the specific design of the converter allows adding all calibration gases upstream of the converter at the inlet tip. An Advanced Pollution Instrumentation (API) UV photometric ozone calibrator was used as transfer standard for calibration of the O_3-channel on ground.

The precision of the NO_y, NO and O_3 data with a resolution of 1 Hz was determined from the fluctuations of the background signal. The accuracy was calculated by taking into account the uncertainties in the calibration gas standards (±4%) and the variation of the mass flow controllers (±2%). For the NO_y-channel the accuracy contains also the uncertainties in the conversion efficiency for different species (±15%), an additional calibration gas uncertainty of (±3.7%), and an experimentally determined pressure correction (±3%). The overall accuracies of the NO_y, NO and O_3 then are ±(0.168·[NO_y]+11 pptv), ±(0.045·[NO]+9 pptv), and ±(0.05·[O_3]+149 pptv), respectively. These specifications refer to a 2σ confidence level.

The NO_y measurement of ECO was compared side-by-side with the NO_y instrument used in the EU program MOZAIC (Paetz et al., 2005[1]) temporally mounted on the Learjet during a dedicated instrument validation flight. The two systems are generally in good agreement with some deviations after calibration and during ascent and descent phases of the aircraft where the differences lie outside the range of the combined stated accuracies.

During the November 2001 and the January 2002 campaigns, an older 1-channel measurement system was used yielding NO_y data only. For completeness O_3 from the Jülich Ozone Experiment JOE with an accuracy of 5% (Mottaghy, 2001) is shown for these two campaigns, while NO_x (=NO+NO_2) data is lacking. Both, JOE and the ECO analyzer showed excellent agreement for the ozone measurements during the other SPURT campaigns (Hegglin, 2004; Engel et al., 2005).

N_2O data were sampled with a Tunable Diode Laser Absorption Spectrometer (TDLAS) with total uncertainty of the measurements of less than ±2% (Hoor et al., 2002).

3. Methods

3.1. Equivalent latitude-potential temperature coordinates

Meridional advection of subtropical air masses or southward excursions of stratospheric polar air associated with Rossby and smaller scale waves lead to deviations of the local tropopause from the climatological mean. At the same time air is advected from regions with higher or lower climatological mean concentrations. These wavy air motions, which are adiabatic to first order and largely reversible, lead to large variability in trace gas distributions in a traditional three-dimensional (longitude, latitude, pressure) coordinate system. In an attempt to remove this variability we therefore use

[1] Paetz, H. W., Volz-Thomas, A., Hegglin, M. I., Brunner, D., Fischer, H., and Schmidt, U.: In-situ comparison of the NO_y instruments flown in MOZAIC and SPURT, in preparation, 2005.

a two-dimensional potential vorticity based equivalent latitude (ϕ_e) and potential temperature (Θ) framework to present our data. This framework follows the meridional deformations in PV contours and uses the fact that PV behaves like a passive tracer under adiabatic and frictionless motions. The equivalent latitude of a PV contour is defined as the latitude of a circle centered about the pole enclosing the same area as the PV contour (Butchart and Remsberg, 1986). This is illustrated in Fig. 1. If $A(PV)$ is the area enclosed by the PV contour, then its equivalent latitude is given by $\phi_e(PV) = \sin^{-1} \cdot (1 - 2 \cdot A(PV))$. For the SPURT measurements the PV-equivalent latitude relationships were calculated for 27 individual isentropes from Θ=270 K up to Θ=400 K in steps of 5 K. In this way we obtained a field $\phi_e(PV, \Theta)$ for discrete values of PV and Θ. The equivalent latitude for each measurement point was then calculated by bilinear interpolation onto the [PV(t), Θ(t)] pairs, where PV(t) and Θ(t) are ECMWF model values interpolated in space ad time onto the flight track coordinates [lon(t), lat(t), p(t)]. Hegglin et al. (2005) used the equivalent latitude-potential temperature framework in a 2-D advection-diffusion model in order to simplify the complexity of atmospheric transport processes and obtained a good approximation of the observed distributions of carbon monoxide in the extratropical LMS.

3.2. Vertical tracer profiles

The vertical distribution of a trace gas species is also strongly influenced by the meteorological situation and in particular by the actual position of the tropopause. Since tropopause heights can vary between several kilometers altitude and simple averaging over height may lead to a smearing out of expected structures in vertical profiles of tracers, the data should be scaled relative to the actual tropopause height. For this purpose, we use the difference between the potential temperature at flight level and at the tropopause ($\Delta\Theta$ from the tropopause) as derived from ECMWF-data. Hoor et al. (2004) showed that the use of $\Delta\Theta$ from the tropopause as vertical coordinate produces less scattering and higher compactness in tracer profiles than the use of absolute potential temperature values. The tropopause used for calculating the profiles

hereafter is defined as the 2 PVU surface.

3.3. Tracer-tracer correlations

Tracer-tracer correlations have been demonstrated to serve as valuable tools for the study of transport processes in the stratosphere and for the validation of CTMs (Bregman et al., 2000) or GCMs (Sankey and Shepherd, 2003). As in the case of the equivalent-latitude concept, the use of a chemical framework removes much of the variability found in tracer time series which are caused by advection of air masses because different long-lived tracers are advected similarly. In this study we focus on the correlations between NO_y and N_2O, O_3 and N_2O, and NO_y and O_3.

NO_y is produced predominantly in the tropical lower stratosphere by the oxidation reaction

$$N_2O + O(^1D) \rightarrow NO + NO \quad (1)$$

which accounts for 5.8% of the total N_2O loss. Highest production rates for NO_y are found in the tropical stratosphere between 25 and 35 km. Since photochemistry is also involved in the production of O_3 in this region, the two tracers are positively correlated with each other. In contrast N_2O is a tropospheric tracer which has its only sink in the stratosphere by photolysis and the reaction with $O(^1D)$. It is therefore negatively correlated with both, NO_y and O_3. Above 40 km, NO_y loss becomes important due to the reaction

$$NO + N \rightarrow N_2 + O \quad (2)$$

and the negative correlation of NO_y with N_2O turns into a positive one. Also the correlation between N_2O and O_3 becomes positive as one exceeds the O_3 maximum above around 30 km. Due to the chemical aging during transport towards the poles and mixing with air masses originating from above the O_3 and NO_y maxima, the slopes of the tracer correlations $\Delta O_3/\Delta N_2O$ and $\Delta NO_y/\Delta N_2O$ show a latitudinal dependency with

ACPD
5, 8649–8688, 2005

larger absolute values in the tropics than at the poles, and intermediate slopes in the mid-latitudinal surf-zone (Bregman et al., 2000; Proffitt et al., 2003).

The tracer correlation between O_3 and N_2O or NO_y and N_2O besides other long-lived species have been widely used to estimate chemical ozone loss, identification of denitrification processes, and characterization of air mass origin (Proffitt et al., 2003, and references therein). However, the here discussed tracer correlations may not be an appropriate tool to identify chemical ozone loss because they may be strongly influenced by transport and mixing processes with chemically aged stratospheric air from above the O_3 or NO_y maxima or with stratospheric air masses from mid-latitudes which also show different correlation-characteristics (Michelsen et al., 1998; Plumb et al., 2000). The SPURT data set offers the opportunity to obtain a seasonally and latitudinally resolved picture of the relationships between different long-lived tracers in the LMS. Questions are whether the linearity and compactness of the tracer-tracer correlations observed in the lower stratosphere are maintained in the LMS or whether STE processes destroy the tight relationships. The degree to which linear correlations are maintained may be useful for interpretation of air mass origin and chemical processing.

4. Results and discussion

In the following we present the data of the long-lived tracers NO_y, N_2O, O_3 and of the shorter-lived NO_x (calculated from measured NO) obtained during the SPURT project by using the above discussed reference systems: Mean distributions in (ϕ_e,Θ)-space for each campaign separately, vertical profiles in $\Delta\Theta$ from the tropopause with focus on the seasonality in the observed trace gas species, and tracer-tracer correlations in order to explore their applicability in the LMS region and to gain insight into the origin of the probed air masses. In Sect. 4.4 finally, the influence of the measured NO mixing ratios on the ozone chemistry is evaluated.

4.1. Median tracer distributions in (ϕ_e, Θ) coordinates

All measurement points are binned into 5° equivalent latitude by 5 K potential temperature bins. For each bin including more than 4 data points, median values were computed. Medians have been used since they are less sensitive to extreme values in a data set than mean values. Figures 2, 3, 4, and 5 show the distributions of median NO_y, N_2O, O_3, and NO_x values during each campaign sorted by month and season. NO_x is the sum of NO and NO_2. The latter has been calculated from the SPURT NO and O_3 mixing ratios using the photostationary equilibrium assumption by Crawford et al. (1996):

$$\frac{[NO]}{[NO_2]} = \frac{J_{NO_2}}{k_1 \cdot [O_3]} \tag{3}$$

with J_{NO_2} being the photolysis rate of NO_2 with dependency on altitude and solar zenith angle for clear-sky conditions. k_1 further is the reaction rate of

$$NO + O_3 \rightarrow NO_2 + O_2. \tag{4}$$

For flights during night time NO_x can not be calculated.

The (ϕ_e,Θ) plots provide an overview of the geographical coverage obtained in each campaign. As shown in Figs. 2 to 5, the SPURT data set achieved a good coverage of the mid-latitude LMS between 35° N and 65° N and below 370 K in mainly every season. During spring campaigns, the best height coverage in $\Delta\Theta$ from the tropopause has been obtained. Only a few tropospheric measurements of NO_y are available for both autumn campaigns due to instrument problems.

We may consider the different campaigns shown in Figs. 2, 3, and 4 as a sequence of months within one year (from January, February, April, May, July, August, October, to November). The result is a seasonal cycle with a smooth change in tracer mixing ratios over the course of a year.

Highest NO_y mixing ratios of around 5 ppbv and O_3 of around 1000 ppbv, together with lowest N_2O of around 265 ppbv are found in the LMS during the spring April

ACPD
5, 8649–8688, 2005

campaign at highest Θ levels and PV-values between 8 and 10. These values decrease gradually towards autumn with a minimum in October, when tracer mixing ratios at these levels were around 2 ppbv NO_y and 500 ppbv O_3. Simultaneously, N_2O values increased towards 310 ppbv.

The observed changes in the mixing ratios can be explained by the seasonality in the strength of the Brewer-Dobson circulation. The stronger the mean meridional circulation, the more O_3 or NO_y is transported from its source region in the tropical lower stratosphere towards higher latitudes and altitudes and then down into the LMS. Simultaneously, lowest N_2O mixing ratios are transported to the LMS. However, the seasonal variation in the net mass flux across the 380 K isentrope and therefore in the strength of the Brewer-Dobson circulation exhibits a maximum in mid-winter and a minimum in late spring early summer (Appenzeller et al., 1996). We observe a shift of the maximum O_3 and NO_y and the minimum N_2O mixing ratios towards April. This is due to the fact that it takes some time to transport the high concentrations from the source region located in the tropics above 380 K to higher latitudes, but also due to the additional time needed to bridge the distance between the 380 K isentrope and the potential temperature at which the measurements have been taken. While the global mean circulation has been shown to dominate the seasonal cycle of long-lived trace gases in the lower stratosphere (Strahan et al., 1999a, b; Garcia et al., 1992), our results show that this dominating influence extends down into the LMS.

In general, tracer mixing ratios of O_3 and N_2O are distributed uniformly in the troposphere, but they exhibit a strong gradient beginning at the tropopause (with PV=2 PVU) and persisting throughout the LMS. NO_y is more variable in the troposphere, but the gradient in the tracer mixing ratios across the tropopause is still obvious. The isopleths of different tracers are closely following the shape of the tropopause similar to the SPURT CO-measurements (Hoor et al., 2004; Hegglin et al., 2005). They show therefore a distribution comparable to the one of potential vorticity. With increasing PV, NO_y and O_3 increase while N_2O decreases resulting in tight positive and negative correlations, respectively. A similar distribution along PV isolines was also found for

H_2O (Krebsbach et al., 2005a, b[2]). However, the tracer isopleths are not strictly parallel to the PV-isolines, i.e. the correlations with PV are different on different isentropes. Furthermore, the relationship is strongly varying with season. Note that pronounced gradients exist both in the vertical across potential temperature levels but also in the horizontal along isentropes. This implies that the extratropical tropopause acts as a barrier to transport and mixing in both, the vertical and the horizontal directions. Vertical transport is hindered by strongly increasing potential temperature, whereas quasi-horizontal transport along isentropes is impeded by increasing PV values in meridional direction (cf. Sect. 4.2). Rather being a distinct barrier to mixing, the tropopause thus appears to define the lower border of a region where mixing is generally suppressed.

The shorter lived tracer NO_x, on the other hand, is much more variable as can be seen in Fig. 5. This is because it has many different local sources and sinks, a relatively short lifetime of about 8 days in the UT/LMS (Jaeglé et al., 1998), and a strong dependency on available sunlight. During the autumn and winter campaigns with little or no sunlight, NO_x mixing ratios are around 0.1 ppbv. At this time of the year, NO_x is mainly converted into its reservoir species such as N_2O_5, HNO_3, or $ClONO_2$. In the presence of sunlight during spring and summer, however, NO_x is reactivated which leads to generally higher mixing ratios with values around 0.3 ppbv. Patches in the observed distributions may be a result of relatively fresh sources of NO_x transported into the LMS after production by lightning or convective uplift of emissions from the planetary boundary layer. These processes have the potential to alter significantly mean NO_y mixing ratios (see Hegglin et al., 2004). Aircraft emissions are another relevant source of NO_x in the mid-latitudinal LMS over Europe.

[2]Krebsbach, M., Brunner, D., Günther, G., Hegglin, M., Spelten, N., and Schiller, C.: Characteristics of the extratropical transition layer as derived from H_2O and O_3 measurements in the UT/LS, Atmos. Chem. Phys. Discuss., to be submitted, 2005b.

4.2. Tracer vertical profiles

Vertical profiles of the measured trace gas species NO_y, N_2O, O_3, and NO_x obtained for each season are shown in Figs. 6 to 8. SPURT campaign data of two different years but corresponding to the same season are shown in the same vertical profile. In order to investigate a possible dependency of the vertical tracer distributions on latitude the data was classified and colored in the figures corresponding to its equivalent latitude into subtropical (ϕ_e<35° N, blue), mid latitudinal (35° N<ϕ_e<65° N, light grey) and polar air masses (ϕ_e>65° N, green). Further, median tracer profiles have been calculated for each season (red lines).

Figures 6a and b show the vertical profiles of N_2O and NO_y for each season. N_2O in general forms relatively compact profiles whereas NO_y shows higher variability. The reason for this is that N_2O is uniformly distributed in the troposphere and has no additional sources in the stratosphere, whereas NO_y has additional sources in the UT/LMS beside its main stratospheric source as discussed above. Figure 7a shows the vertical profiles for O_3. Interestingly, the same qualitative features as found for NO_y are also seen in the O_3 profiles. Upper tropospheric mixing ratios of NO_y and O_3 are higher in spring and summer than in autumn and winter by about 100% and 60%, respectively. The same seasonality has been obtained by Krebsbach et al. (2005a) using 2-D probability distribution functions for O_3.

In the autumn panels of each figure, the vertical profiles of all seasons are shown together for comparison. The most obvious feature is a uniform distribution of the tracers in the troposphere and a strong gradient in the tracer mixing ratios beginning at around 5 K below the tropopause (with PV=2 PVU) as stated in the previous section. The gradients in the tracer profiles of NO_y, N_2O, and O_3 found across the tropopause (see Figs. 6a, b and 7a) are strongest in spring, decreasing throughout summer towards lowest gradients in autumn and increasing again during winter towards spring values. As can be seen in Fig. 7b, there is also a strong gradient in PV of 1 PVU/5 K between −10 K and 30 K above the tropopause. Above 30 K the PV gradient becomes smaller

ACPD
5, 8649–8688, 2005

again. Our results agree with recent evaluations of the static stability in the tropopause region by Birner (2005)[3]. The strong change in PV and with it the change in static stability may act as a transport barrier to mixing causing the observed gradients in the different tracers. Interestingly, PV shows the same gradient in all seasons, while the gradients in the observed chemical tracers show a strong seasonal dependency. This may be explained by a change in the supply of the tracers from the stratospheric overworld which is dependent on the strength of the Brewer-Dobson circulation as discussed in Sect. 4.1. Also, the origin of the air masses is relevant since air from above 380 K is not purely aged stratospheric air but is rather a mixture containing also younger air from the tropical tropopause region (cf. Hoor et al., 2005). This topic will be investigated in the next section. The Brewer-Dobson circulation further acts to remove tropospheric air transported into the LMS by troposphere-to-stratosphere transport (TST) at the extratropical tropopause. The effect of TST events further seems to be smoothed out by fast horizontal transport and mixing in the zonal direction as has been previously suggested by Hegglin et al. (2005) and Birner (2005)[3]. The result is a gradual transition from the troposphere into the stratosphere referred to as the extratropical tropopause transition layer. In summer the low gradient within this tropopause layer is therefore explained by both, a weaker Brewer-Dobson circulation and stronger tropospheric influence, filling up the LMS with tropospheric air as time proceeds towards autumn.

The vertical profiles of the shorter lived NO_x for each season are finally shown in Fig. 8. In winter and autumn the vertical gradients in NO_x together with the variability in NO_x is relatively low. In spring and summer, however, a strong gradient exists across the tropopause and a bulge in the vertical profiles characterized by higher variability and higher NO_x mixing ratios is obvious between −10 K and 30 K above the tropopause. This feature is likely due to a combination of the increase in available sunlight enhancing NO_x by photolysis of HNO_3, an increase in deep convection associated with lightning production of NO towards summer, and a weakening of the

[3]Birner, T.: The fine-scale structure of the extratropical tropopause region, J. Geophys. Res., submitted, 2005.

Brewer-Dobson circulation replacing less lowermost stratospheric air influenced by STE processes or local aircraft emissions. The low temperatures and low O_3 mixing ratios found in the tropopause region may further slow down chemical reaction rates of heterogeneous and gas-phase conversion of NO_x into its reservoir species.

The classification of the air masses corresponding to their equivalent latitude (blue, light grey, green data points) suggests that tracer profiles of NO_y, N_2O, and O_3 show no significant latitudinal dependency except in summer. The mixing ratios are mainly determined by their vertical distance relative to the tropopause and are similar for subtropical, mid latitude and polar air masses. In summer, however, mixing ratios of NO_y and O_3 tend to be higher and lower for N_2O in the polar region compared to values measured in the subtropics indicating a reservoir of older air at higher latitudes. It is interesting to see that the latitudinal gradient in potential vorticity is also most pronounced in summer (Fig. 7b). This suggests that mixing and transport within the lowermost stratosphere which tend to smooth out latitudinal gradients are slower than time scales of processes which provide the lowermost stratosphere with tropospheric air starting in the beginning of summer and at lower latitudes. The latter may be associated with deep convective events which could also explain the highly variable NO_x found in summer in the first 20 K above the tropopause. NO_x also reveal a stronger dependency on ϕ_e than the other tracers during all seasons. Higher mixing ratios are found in regions south from 35° N, while lower values are found at higher ϕ_e. However, more measurements and probably over an even broader range of ϕ_e and Θ should be carried out to better characterize the latitudinal tracer gradients.

4.3. Seasonality of tracer-tracer correlations

Figure 9 shows the correlation plots of O_3 with N_2O obtained during the different campaigns. For each data set, the correlation between O_3 and N_2O has been calculated by using stratospheric data points only with potential vorticity >2 PVU. In general, the correlations between the two tracers are quite compact and near-linear yielding correlation coefficients (R^2) between 0.79 and 0.96 and indicating that the air masses in this

region of the LMS are well mixed. Correlations have also been calculated for scatter plots between NO_y and N_2O but using only data points with O_3 mixing ratios >300 ppbv in order to exclude air masses which show high variability in NO_y due to tropospheric sources. The NO_y and N_2O scatter plots are less compact (not shown). Correlation coefficients (R^2) for May 2002, February, April, and July 2003 campaigns are between 0.6 and 0.73, but smaller than 0.4 for the other campaigns. The more compact correlations found between February and July suggest that the LMS is dominated during winter and spring by stratospheric air masses. On the other hand, the influence of the troposphere across the extratropical tropopause appears to become strongest between August and November, leading to less compact correlations between NO_y and N_2O (see Hegglin, 2004).

For both tracer-tracer combinations, the correlations obtained in different years but corresponding to the same season show similar average slopes ($\Delta O_3/\Delta N_2O$ and $\Delta NO_y/\Delta N_2O$). In Fig. 10b and c, the obtained correlation slopes are plotted as a function of time. The SPURT data set suggests, that the correlation slopes follow a seasonal cycle indicated by the red lines. The slopes of the NO_y to N_2O correlation show changes between October 2002 and February 2003 of 15%. This result is significantly higher than the change in slope observed in ER2-data above 400 K during the ASHOE/MAESA and STRAT campaigns being around 7% (Keim et al., 1997). The difference of the two observations may be explained by inter-annual variability in the strength of the mean meridional circulation which determines the amount of aged stratospheric air transported towards the LMS.

The seasonal cycle in the correlation slopes may be explained by the Brewer-Dobson circulation as seen in Sect. 4.1 and indicates furthermore changing air mass origin. Fahey et al. (1990) presented the distribution of $\Delta NO_y/\Delta N_2O$ ratios in the lower stratosphere calculated by a 2-D chemical transport model and showed that high absolute values are found in the tropical lower stratosphere, whereas low absolute values are found in higher altitudes and latitudes. Bregman et al. (2000) further analyzed the $\Delta O_3/\Delta N_2O$ ratios within the lower stratosphere obtained by a 3-D chemical transport

model and found a latitudinal dependency with decreasing absolute values towards higher latitudes. They both explained their findings by the combined effects of transport and chemistry. Small absolute values of both, $\Delta O_3/\Delta N_2O$ and $\Delta NO_y/\Delta N_2O$ as found during spring in our study suggest that these air masses originate from higher altitudes and latitudes being either chemically processed on their way to higher latitudes and during descent in the polar vortex or being influenced by air descending from altitudes above 35–40 km where the linear relationships between the discussed tracers reverses sign. On the other hand, large absolute values of the correlation slopes as found during autumn represent younger air masses typical for the tropical lower stratosphere region and which took a 'shorter' pathway leading more directly from the tropical tropopause to the LMS region. These findings are in close agreement with Hoor et al. (2005) who showed that the contribution of tropical tropospheric air to the chemical composition of the LMS amounts to about 35% in spring, while in autumn the contribution is about 55%. Winter and summer represent intermediate stages.

The observed seasonal cycle in the correlation slopes is roughly in phase with the downward mass flux calculated by Appenzeller et al. (1996) shown in Fig. 10d. The largest mass fluxes across a reference surface (e.g. the 380 K isentrope) coincide with the steepest correlation slopes, while smaller mass fluxes found in spring are coincident with more shallow slopes. The largest fraction of aged stratospheric air in the LMS therefore is found at the end of a period with strong downward mass transport. As noted above, correlation slopes found between tracers in the LMS may also be influenced by the inter-annual variability in the strength of the Brewer-Dobson circulation and therefore tracer measurements may be used in future as a valuable measure of the circulation strength.

It is interesting to note, that the slopes of the NO_y to O_3 correlation show no significant seasonal cycle (see Fig. 10a). The explanation for this may be that the two species are linearly correlated throughout the stratosphere and mixing with air masses of above the NO_y and O_3 maxima does not lead to a change in the correlation slope.

The SPURT data presented here do not allow to decide whether the observed slopes

during spring and summer are the result of mixing with air masses which experienced enhanced chemical ozone loss and denitrification or whether they result from transport and mixing processes with air above the O_3 and NO_y maxima where different correlation-characteristics prevail (Michelsen et al., 1998; Plumb et al., 2000; Proffitt et al., 2003). For this purpose other tracer-tracer correlations e.g. between CH_4 and N_2O can be used, which are not influenced by chemical processes. Since the dynamical range of the SPURT CH_4 data was not large enough to obtain compact correlations we were not able to look into this in more detail. Nevertheless, the vertical profiles of the CH_4 mixing ratios (not shown) also exhibit a seasonal cycle similar to what has been seen in Figs. 6a, b and 7a, suggesting that rather the origin of air than enhanced chemical processing influences the observed tracer distributions in the LMS.

4.4. Chemical regime: ozone destruction or production

The chemical composition and the physical characteristics of the UT/LMS together with the influence of complex dynamical processes on smaller and larger scales, make this region difficult to simulate in global chemical transport models (Brunner et al., 2003). In particular, large differences between modelled and measured NO_x ask for a more accurate description of NO_x sources such as lightning and deep convection and consequent transport into the LMS. The good coverage of the UT/LMS with highly resolved tracer measurements including the key species for ozone chemistry (NO and CO) as obtained during SPURT allow to determine at which height the chemical regime switches from O_3 production to O_3 destruction.

Figure 11 shows schematically the dependence of net O_3 production available NO and on background O_3 mixing ratios as well as the NO^{crit} value at which O_3 destruction turns into O_3 production (indicated by the red lines). It reproduces the results by Grooss et al. (1998) using the Mainz two-dimensional photochemical model for upper tropospheric conditions, where the NO^{crit} value increases with increasing O_3 mixing ratios from values around 0.01 ppbv at 50 ppbv O_3 to 0.1 ppbv at 200 ppbv O_3. They

further showed that decreasing values of CO result in a decrease in peak net O_3 production, but has no influence on NO^{crit}. Finally, volatile organic compounds may be neglected in a first approximation, since Grooss et al. (1998) showed that the reaction of $NO+HO_2$ dominates the O_3 production. It becomes obvious from Fig. 11 that net O_3 production is highly non-linear below and above the critical NO mixing ratio. It is therefore important to know which chemical regime prevails in order to assess the chemical impact of additional NO_x sources such as aircraft emissions and lightning production on UT/LMS O_3 chemistry and its impact on climate.

We calculated for each season vertical profiles of the critical NO mixing ratios (NO^{crit}) below which O_3 destruction takes place assuming that the following chemistry prevails:

$$OH + O_3 \rightarrow HO_2 + O_2 \qquad k_1 \tag{5}$$

$$OH + CO \rightarrow H + CO_2 \qquad k_2 \tag{6}$$

$$HO_2 + NO \rightarrow NO_2 + OH \qquad k_3 \tag{7}$$

$$HO_2 + O_3 \rightarrow OH + 2\,O_2 \qquad k_4 \tag{8}$$

with k_1 to k_4 being pressure or temperature dependent reaction rates taken from Brasseur and Solomon (1986). The temporal change in O_3 then is given by

$$\frac{d[O_3]}{dt} = -k_1[OH][O_3] - k_4[HO_2][O_3] + k_3[HO_2][NO] \tag{9}$$

and the temporal change in OH by

$$\frac{d[OH]}{dt} = -k_1[OH][O_3] - k_2[OH][CO] + k_3[HO_2][NO] + k_4[HO_2][O_3]. \tag{10}$$

Imposing steady state onto both Eqs. (9) and (10) followed by some rearrangements and the replacement of the ratio [OH]:[HO_2] in Eq. (9) yields the expression for the

critical NO value

$$[NO]^{crit} = \frac{k_4}{k_3} \cdot [O_3] \cdot \left(1 + \frac{2k_1[O_3]}{k_2[CO]}\right). \quad (11)$$

In the troposphere where $2k_1[O_3] \ll k_2[CO]$, the term in the brackets in Eq. (11) approximates 1 and the calculation for $[NO]^{crit}$ gets equal to the one derived by Crutzen (1979) for use in the troposphere. Our derivation of NO^{crit} suggests, that changing CO mixing ratios have a significant impact on NO^{crit} in contrast to the results of Grooss et al. (1998). Finally, if measured NO exceeds the calculated critical NO-mixing ratio chemical conditions favor O_3 production. If measured NO is lower than NO^{crit}, O_3 destruction is expected.

Figure 12 shows the calculated mean NO^{crit} values dependent on the distance $\Delta\Theta$ from the tropopause for each season. The NO^{crit} values show a seasonal cycle with highest values in spring and lowest in autumn. This is explained by its dependence on the background O_3 mixing ratios which show also a maximum in spring and a minimum during autumn. Measured NO mixing ratios in winter exceed the calculated NO^{crit} values up to 20 K above the tropopause. This height is 30 K during spring and increases to around 40 K during summer and 50 K during autumn. The profiles reveal also a latitudinal dependency. Data measured North from 65° N show an atmospheric composition which favors O_3 destruction, whereas the data measured at latitudes South from 35° N favor O_3 production.

The results of our study indicate that the chemical regime in the UT/LMS is dependent on season and that it favors photochemical O_3 production up to a maximum height of $\Delta\Theta$=50 K above the tropopause during autumn. Koch et al. (2002) found positive O_3 trends in the UT/LMS region depending on season and reaching maximum altitudes in autumn. According to our study, chemical production may serve as an explanation for these trends assuming a positive trend would also exist in available NO. While the next step should be the quantification of the net O_3 production by using a more complex chemistry model including all important reactions in the tropopause region, the here

presented results may be useful to validate the chemical regime obtained in global chemistry transport models.

5. Conclusions

A new measuring system for high resolution and high sensitivity measurements of NO_y, NO, and O_3 was implemented into a Learjet 35A aircraft. The measurements were performed simultaneously using a three-channel chemiluminescence detector and an externally mounted converter in which NO_y species were reduced catalytically to NO on a heated gold surface in the presence of CO. The semi-automated system was successfully operated during a total of six measurement campaigns plus two campaigns with an older system performed seasonally between November 2001 and July 2003 in the framework of the SPURT project. The mission flights covered the region of the upper troposphere and LMS over Europe from 30° to 75° N up to a potential temperature of 370 K.

The SPURT measurements presented in the equivalent latitude - potential temperature framework reveal that tracer distributions of NO_y, N_2O, and O_3 in the LMS show relatively simple features with a gradual increase in mixing ratios with increasing distance from the tropopause and a strong dependency on season. Tracer gradients exist in the vertical across isentropes but also in the horizontal along isentropes. The tracer distributions in winter and spring are characterized by high NO_y and O_3, and low N_2O mixing ratios, whereas in summer and autumn, N_2O mixing ratios are close to tropospheric values and O_3 and NO_y mixing ratios are low. This seasonal change reveals a clear influence of the Brewer-Dobson circulation on the LMS. NO_x abundances finally are dependent on available sunlight and therefore show enhanced values in spring and summer.

Vertical profiles of all the tracers show a strong gradient across the tropopause simultaneously with a strong gradient in potential vorticity (PV) of 1 PVU/5 K that may act as transport barrier. Latitudinal differences are absent except in summer, indicating no

ACPD
5, 8649–8688, 2005

additional transport barriers within the LMS. These findings agree well with dynamical observations (Birner, 2005[3]). The latitudinal gradient found in summer may in turn be a result of the period during which the LMS is being 'filled up' with tropospheric air by different troposphere-to-stratosphere transport processes.

Scatter plots between O_3 and N_2O and between NO_y and N_2O obtained during SPURT show compact correlations implying that the concept of tracer-tracer correlations may also be used within the LMS to determine origin or chemical aging of air masses. There is one restriction to be made. In the case of NO_y and N_2O, only data points should be used which lie above around 300 ppbv O_3 below which NO_y can be highly perturbed by troposphere-to-stratosphere transport processes which then may alter the calculated correlation slopes significantly. For tracers which are well-mixed in the troposphere, however, the compactness is given throughout the LMS. The correlations between NO_y and N_2O as well as between O_3 and N_2O reveal pronounced seasonal cycles, being in phase with the calculated mass fluxes across the 380 K isentrope derived by Appenzeller et al. (1996). The changing slope values offer insight into the origin of the air masses. While in spring the correlation slopes $\Delta NO_y/\Delta N_2O$ and $\Delta O_3/\Delta N_2O$ indicate that aged stratospheric air, i.e. air which travelled through high altitudes and/or high latitudes and probably descended in the polar vortex, determines the background air of the lowermost stratosphere, in autumn the air may have taken a 'shorter' pathway leading more directly from the tropical tropopause region to the LMS. The fact that the NO_y to N_2O ratio is strongly dependent on season must be accounted for when calculating excess NO_y, a value which helps to determine additional sources of NO_y in the LMS. The slope of the correlation between NO_y and O_3, on the other hand, is variable from year to year.

The SPURT NO measurements provide highly resolved measurements of key species involved in O_3 chemistry. In this study we calculated height-dependent critical NO values (NO^{crit}) which determine the crossover point between O_3 production and destruction. Measured NO lying above the calculated NO^{crit} values and favoring O_3 production were found in every season within the extratropical tropopause transi-

tion layer. While in winter the O_3 production regime reaches up to 20 K above the local tropopause, it increases over spring and summer and reaches up to 50 K above the tropopause in autumn. High latitudes show more data points lying in the O_3 destruction regime, most probably because less solar radiation is available for the photochemical reactions being responsible for the O_3 production.

The SPURT data set finally represents a valuable contribution to a global climatology of NO_y, N_2O, NO, and O_3 among other long-lived species. Through the specific campaign setup, the measurements provide both, representative information on long-lived tracer distributions as well as insight into individual processes shaping the chemical structure of the tropopause region (cf. Hegglin et al., 2004). Therefore the data set is an ideal basis on which different issues concerning transport and mixing processes in the tropopause region can be addressed. It may be useful in particular for validation of transport and mixing processes in the UT/LMS in global chemistry transport models or of satellite measurements.

Acknowledgements. The authors would like to thank the firm enviscope GmbH, Frankfurt (Germany) for the professional implementation and operation of the scientific payload, and the GFD (Gesellschaft für Flugzieldarstellung) for their great cooperation and expert support. The SPURT project has been funded by the German BMBF (Bundesministerium für Bildung und Forschung) and the here presented measurements supported by the SNF (Swiss National Fund). Special thanks for useful discussions to I. Folkins, K. Bowman and R. Salawitch.

References

Appenzeller, C., Holton, J. R., and Rosenlof, K. H.: Seasonal variation of mass tranpsort across the tropopause, J. Geophys. Res., 101, 15 071–15 078, 1996.

Baehr, J., Schlager, H., Ziereis, H., Stock, P., van Velthoven, P., Busen, R., Ström, J., and Schuhmann, U.: Aircraft observations of NO, NO_y, CO, and O_3 in the upper troposphere from 60° N to 60° S – Interhemispheric differences at midlatitudes, Geophys. Res. Lett., 30, (11), 1598, doi:10.1029/2003GL016935, 2003.

Brasseur, G. and Solomon, S.: Aeronomy of the Middle Atmosphere, D. Reidel, Norwell, Mass., USA, p. 452, 1986.
Bregman, B., Lelieveld, J., van de Broek, M., Siegmund, P., Fischer, H., and Bujok, O.: N_2O and O_3 relationship in the lowermost stratosphere: A diagnostic for mixing processes as represented by a three-dimensional chemistry-transport model, J. Geophys. Res., 105, 17 279–17 290, 2000.
Brunner, D., Staehelin, J., Jeker, D., Wernli, H., and Schumann, U.: Nitrogen oxides and ozone in the tropopause region of the Northern Hemisphere: Measurements from commercial aircraft in 1995/96 and 1997, J. Geophys. Res., 106, 27 673–27 699, 2001.
Brunner, D., Staehelin, J., Rogers, H. L., et al.: An evaluation of the performance of chemistry transport models by comparison with research aircraft observations. Part 1: Concepts and overall model performance, Atmos. Chem. Phys., 3, 1609–1631, 2003, SRef-ID: 1680-7324/acp/2003-3-1609.
Butchart, N. and Remsberg, E. E.: The area of the stratospheric polar vortex as a diagnostic tracer for transport on an isentropic surface, J. Atmos. Sci., 45, 1319–1339, 1986.
Crawford, J., Davis, D., Chen, G., et al.: Photostationary state analysis of the NO_2-NO system based on airborne observations from the western and central north pacific, J. Geophys. Res., 101, 2053–2072, 1996.
Crutzen, P.: The role of NO and NO_2 in the chemistry of the troposphere and the stratosphere, Ann. Rev. Earth Planet. Sci., 7, 443–472, 1979.
Emmons, L. K., Hauglustaine, D. A., Müller, J.-F., Carrol, M. A., Brasseur, G. P., Brunner, D., Staehelin, J., Thourit, V., and Marenco, A.: Data composites of airborne observations of tropospheric ozone and its precursors, J. Geophys. Res., 105, 20 497–20 538, 2000.
Engel, A., Bönisch, H., Brunner, D., et al.: Highly resolved observations of trace gases in the lowermost stratosphere and upper troposphere from the Spurt project: an overview, Atmos. Chem. Phys. Discuss., 5, 5081–5126, 2005, SRef-ID: 1680-7375/acpd/2005-5-5081.
Fahey, D. W., Eubank, C. S., Hubler, G., and Fehsenfeld, F. C.: Evaluation of a catalytic reduction technique for the measurement of total reactive odd-nitrogen NO_y in the atmosphere, J. Atmos. Chem., 3, 435–468, 1985.
Fahey, D., Solomon, S., Kawa, S., Loewenstein, M., Podolske, J., Strahan, S., and Chan, K.: A diagnostic for denitrification in the winter polar stratosphere, Nature, 345, 698-702, 1990.
Fontijn, A., Sabadell, A., and Ronco, R.: Homogenous chemiluminescent measurement of nitric

oxide with ozone, Angewandte Chemie, 42, 575–579, 1970.
Forster, P. and Shine, K.: Radiative forcing and temperature trends from stratospheric ozone changes, J. Geophys. Res., 105, 10 169–10 857, 1997.
Garcia, R., Stordal, F., Solomon, S., and Kiehl, J.: A new numerical model of the middle atmosphere, 1. Dynamics and transport of tropospheric source gases, J. Geophys. Res., 97, 12 967–12 991, 1992.
Grooss, J. U., Brühl, Ch., and Peter, Th.: Impact of aircraft emissions on tropospheric and stratospheric ozone. Part I: Chemistry and 2-D model results, Atmos. Environ., 32, 3173–3184, 1998.
Hegglin, M. I., Brunner, D., Wernli, H., et al.: Tracing troposphere-to-stratosphere transport above a mid-latitude deep convective system, Atmos. Chem. Phys., 4, 741–756, 2004, SRef-ID: 1680-7324/acp/2004-4-741.
Hegglin, M. I.: Airborne NO_y-, NO- and O_3-measurements during SPURT: Implications for atmospheric transport, Disseration, Eidgenössische Technische Hochschule ETH Zürich, Nr. 15553, URL: http://e-collection.ethbib.ethz.ch/show?type=diss&nr=15553, 2004.
Hegglin, M. I., Brunner, D., Peter, T., Staehelin, J., Wirth, V., Hoor, P., and Fischer, H.: Determination of eddy-diffusivity in the lowermost stratosphere, Geophys. Res. Lett., 32, L13812, doi:10.1029/2005GL022495, 2005.
Holton, J., Haynes, P., McIntyre, M., Douglass, A., Rood, R., and Pfister, L.: Stratosphere-troposphere exchange, Rev. Geophys., 33, 403–439, 1995.
Hoor, P., Fischer, H., Lange, L., and Lelieveld, J.: Seasonal variations of a mixing layer in the lowermost stratosphere as identified by the CO-O_3 correlation from in situ measurements, J. Geophys. Res., 107, D5–D6, 4044, doi:10.1029/2000JD000289, 2002.
Hoor, P., Gurk, C., Brunner, D., Hegglin, M. I., Wernli, H., and Fischer, H.: Seasonality and extent of extratropcial TST derived from in-situ CO measurements during SPURT, Atmos. Chem. Phys., 4, 1427–1442, 2004, SRef-ID: 1680-7324/acp/2004-4-1427.
Hoor, P., Fischer, H., and Lelieveld, J.: Tropical and extratropical tropospheric air in the lowermost stratosphere over Europe: A CO-based budget, Geophys. Res. Lett., 32, L07802, doi:10.1029/2004GL022018, 2005.
IPCC (Intergovernmental Panel on Climate Change): Aviation and the globale atmosphere, edited by: Penner, J. E., Lister, D. H., Griggs, D. J., Dokken, D. J., and McFarland, M., Cambridge University Press, New York, 29–64, 1999.

Jaeglé, L., Jacob, D. J., Wang, Y., Weinheimer, A. J., Ridley, B. A., Campos, T. L., Sachse, G. W., and Hagen, D. E.: Sources and chemistry of NO_x in the upper troposphere over the United States, Geophys. Res. Lett., 25, 1705–1708, 1998.

James, P., Stohl, A., Forster, C., Eckhardt, S., Seibert, P., and Frank, A.: A 15-year climatology of stratosphere-troposphere exchange with a Lagrangian particle dispersion model, part B, Mean climate and seasonal variability, J. Geophys. Res., 108, D12, doi:10.1029/2002JD002639, 2003.

Keim, E., Loewenstein, M., Podolske, J., et al.: Measurements of the NO_y-N_2O correlation in the lower stratosphere: Latitudinal and seasonal changes and model comparisons, J. Geophys. Res., 102, 13 193-13 229, 1997.

Koch, G., Wernli, H., Staehelin, J., and Peter, T.: A Lagrangian analysis of stratospheric ozone variability and long-term trends above Payerne (Switzerland) during 1970–2001, J. Geophys. Res., 107, 4373, doi:10.1029/2001JD001550, 2002.

Kondo, Y., Koike, M., Kawakami, S., Singh, H. B., Nakajima, H., Gregory, G. L., Blake, D. R., Sachse, G. W., Merrill, J. T., and Newell, R. E.: Profiles and partitioning of reactive nitrogen over the Pacific Ocean in winter and early spring, J. Geophys. Res., 102, 28 405–28 424, 1997.

Krebsbach, M., Brunner, D., Günther, G., Hegglin, M., Maser, R., Mottaghy, D., Riese, M., Spelten, N., Wernli, H., and Schiller, C.: Seasonal cycles and variability of O_3 and H_2O in the UT/LMS during SPURT, Atmos. Chem. Phys. Discuss., 5, 7247–7282, 2005a, SRef-ID: 1680-7375/acpd/2005-5-7247.

Lacis, A. A., Wuebbles, D. J., and Logan, J. A.: Radiative forcing of climate by changes in the vertical distribution of ozone, J. Geophys. Res., 95, 9971–9981, 1990.

Lange, L., Fischer, H., Parchatka, U., Gurk, C., Zenker, T., and Harris, G.: Characterization and application of an externally mounted catalytic converter for aircraft measurements of NO_y, Rev. Sci. Instrum., 73, 3051–3057, 2002.

Michelsen, H. A., Manney, G. L., Gunson, M. R., and Zander, R.: Correlations of stratospheric abundances of NO_y, O_3, N_2O, and CH_4 derived from ATMOS measurements, J. Geophys. Res., 103, D21, 28 347–28 359, 1998.

Mottaghy, D.: Aufbau, Charakterisierung und Validierung eines in-situ Instrumentes zur Messung von Ozon in der oberen Troposphäre und unteren Stratosphäre, Diploma thesis, RWTH Aachen, 2001.

Plumb, R. A., Waugh, D. W., and Chipperfield, M. P.: The effects of mixing on tracer relation-

ships in the polar vortices, J. Geophys. Res., 105, D8, 10 047–10 062, 2000.
Proffitt, M. H., Aikin, K., Tuck, A. F., Margitan, J. J., Webster, C. R., Toon, G. C., and Elkins, J. W.: Seasonally averaged ozone and nitrous oxide in the Northern Hemisphere lower stratosphere, J. Geophys. Res., 108, D3, 4110, doi:10.1029/2002JD002657, 2003.
Ridley, B. and Howlett, L.: An instrument for NO measurements in the stratosphere, Rev. Sci. Instrum., 45, 742–746, 1974.
Sankey, D. and Shepherd, T. G.: Correlations of long-lived chemical species in a middle atmosphere general circulation model, J. Geophys. Res., 108, D16, 4494, doi:10.1029/2002JD002799, 2003.
Singh, H. B., Chen, Y., Gregory, G. L., Sachse, G. W., Talbot, R., Blake, D. R., Kondo, Y., Bradshaw, J. D., Heikes, B., and Thornton, D.: Trace chemical measurements from the northern midlatitude lowermost stratosphere in early spring: Distributions, correlations, and fate, Geophys. Res. Lett., 24, 127–130, 1997.
Sprenger, M. and Wernli, H.: A northern hemispheric climatology of cross-tropopasue exchange for the ERA15 time period (1979–1993), J. Geophys. Res., 108, D12, 8521, doi:10.1029/2002JD002636, 2003.
Strahan, S., Loewenstein, M., and Podolske, J.: Climatology and samll-scale structure of lower stratospheric N_2O based on in situ observations, J. Geophys. Res., 104, 2195–2208, 1999a.
Strahan, S.: Climatologies of lower stratospheric NO_y and O_3 and correlations with N_2O-based on in situ observations, J. Geophys. Res., 104, 30 463–30 480, 1999b.
Volz-Thomas, A., Berg, M., Heil, T., Houben, N., Lerner, A., Petrick, W., Raak, D., and Päetz, H.-W.: Measurements of total odd nitrogen (NO_y) aboard MOZAIC in-service aircraft: instrument design, operation and performance, Atmos. Chem. Phys., 5, 583–595, 2005, SRef-ID: 1680-7324/acp/2005-5-583.
Wernli, H. and Bourqui, M.: A Lagrangian "1-year climatology" of (deep) cross tropopause exchange in the extratropical Northern Hemisphere, J. Geophys. Res., 107, D1–D2, 4021, doi:10.1029/2001JD000812, 2002.
Ziereis, H., Schlager, H., Fischer, H., Feigl, C., Hoor, P., Marquardt, R., and Wagner, V.: Aircraft measurements of tracer correlations in the Arctic subvortex region during the Polar Stratospheric Aerosol Experiment (POLSTAR), J. Geophys. Res., 105, 24 305–24 313, 2000.

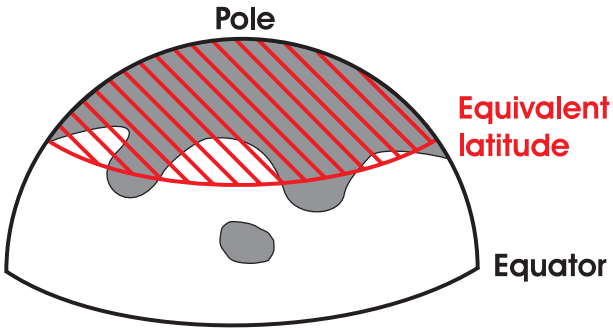

Fig. 1. Sketch illustrating the concept of equivalent latitude (ϕ_e). An area (grey colored) enclosed by a PV-contour on a given isentrope is transformed into a circle centered about the pole of equal area (red hatched). The latitude of this circle is defined as ϕ_e. By using its ϕ_e, a cut-off low with high PV at mid-latitudes and on a given isentrope is moved back to higher latitudes.

ACPD
5, 8649–8688, 2005

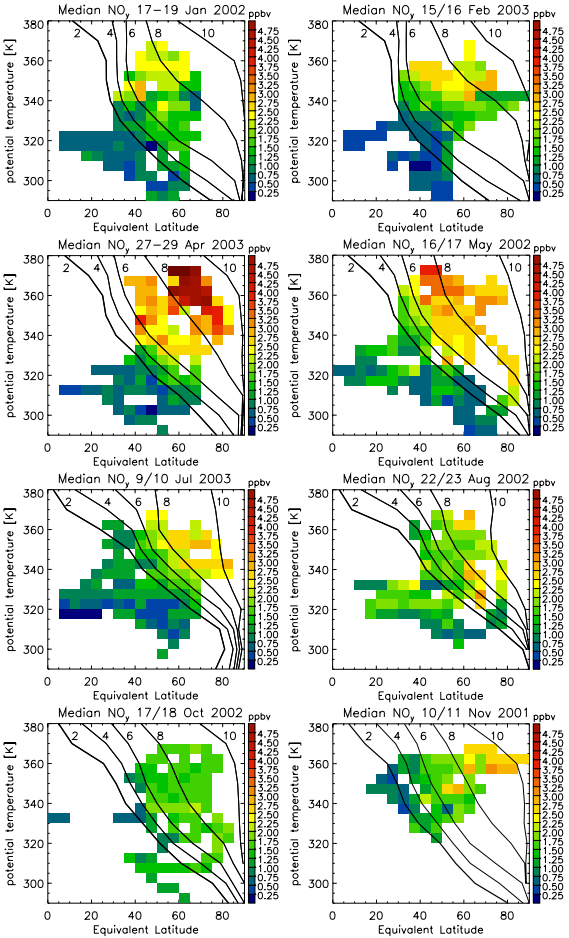

Fig. 2. Median NO_y mixing ratios in (ϕ_e,Θ) coordinates. From top to bottom: winter, spring, summer, and autumn measurements. Black lines denote PV-isolines (2, 4, 6, 8, and 10 PVU). The contour with 2 PVU indicates the dynamical tropopause.

ACPD
5, 8649–8688, 2005

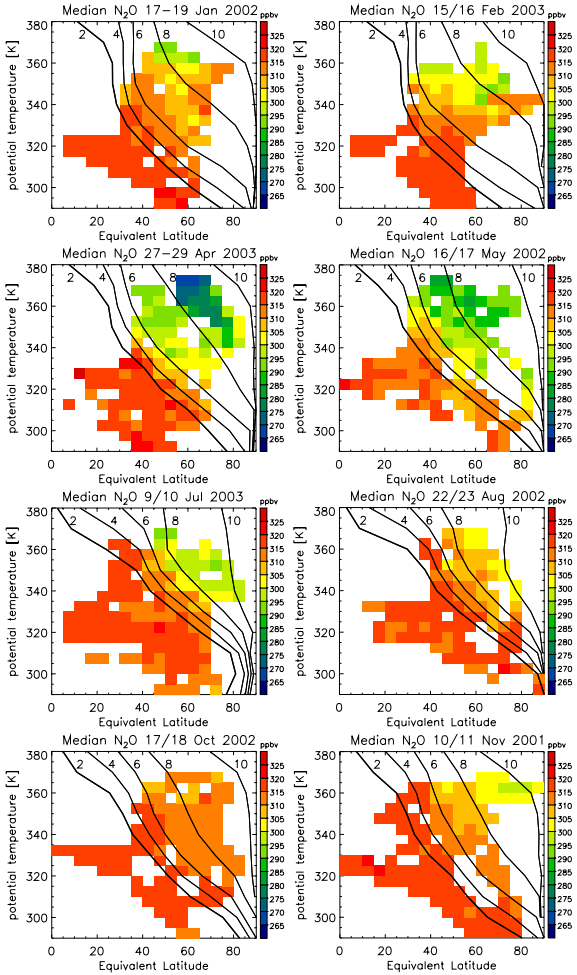

Fig. 3. Same as Fig. 2, but for N_2O.

ACPD
5, 8649–8688, 2005

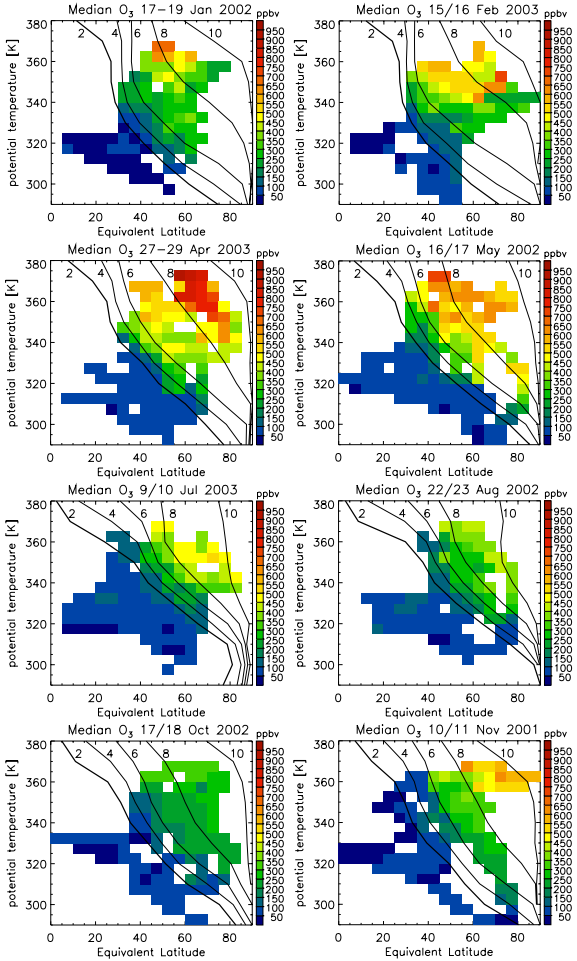

Fig. 4. Same as Fig. 2, but for O_3.

ACPD
5, 8649–8688, 2005

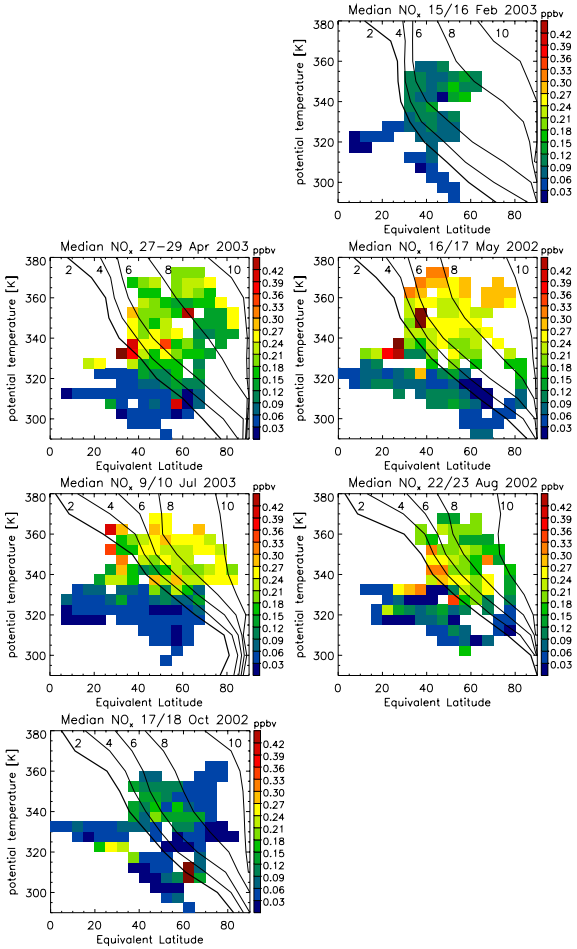

Fig. 5. Same as Fig. 2, but for $NO_x(=NO+NO_2)$.

ACPD
5, 8649–8688, 2005

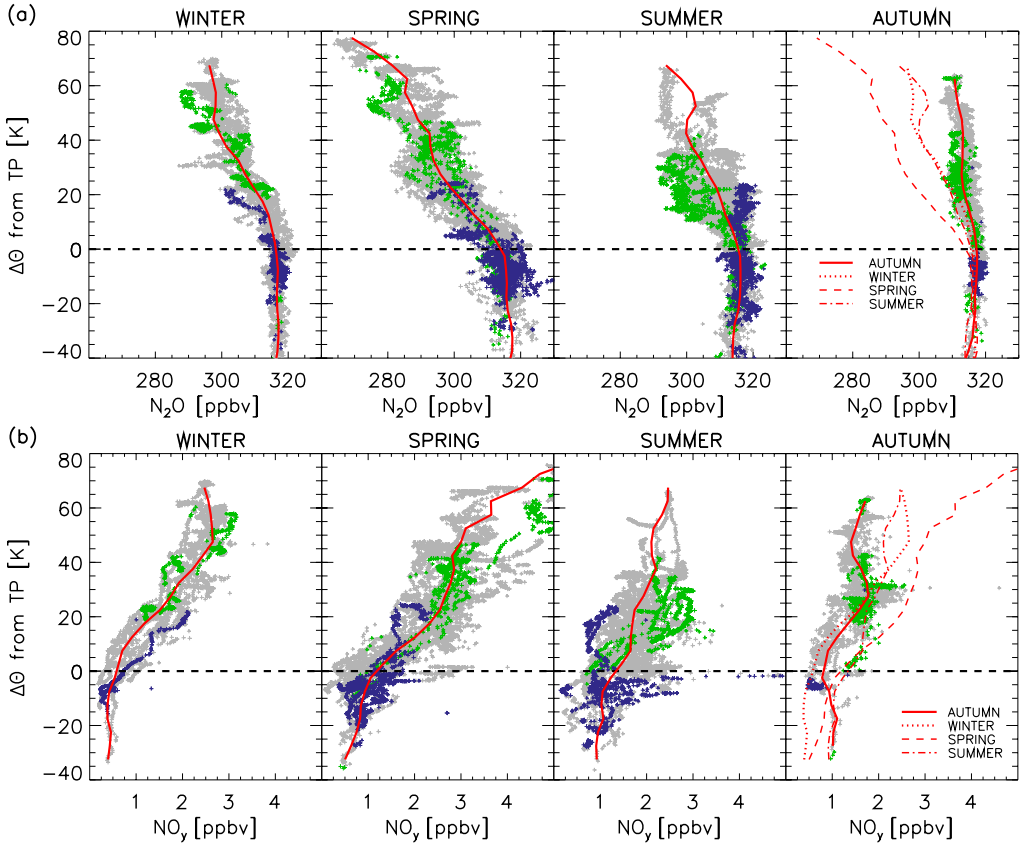

Fig. 6. Vertical profiles of **(a)** N_2O and **(b)** NO_y mixing ratios as a function of $\Delta\Theta$ from the tropopause (defined by 2 PVU). Blue crosses denote measurements with ϕ_e south from 35° N, light grey crosses with ϕ_e between 35° N and 65° N, and green crosses with ϕ_e north from 65° N. Red lines denote profiles of median mixing ratios. To allow direct comparison, the winter, spring and summer profiles are plotted in the autumn graph again.

ACPD
5, 8649–8688, 2005

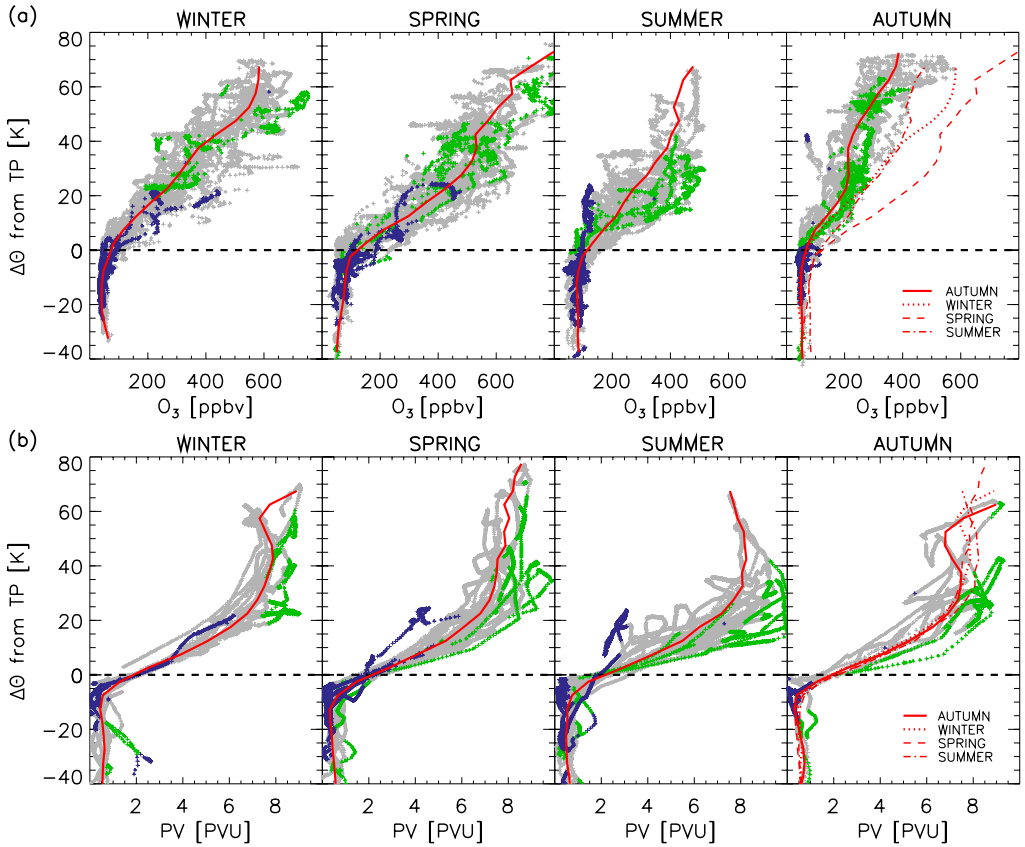

Fig. 7. Same as Fig. 6, but for **(a)** O_3 and **(b)** PV.

ACPD
5, 8649–8688, 2005

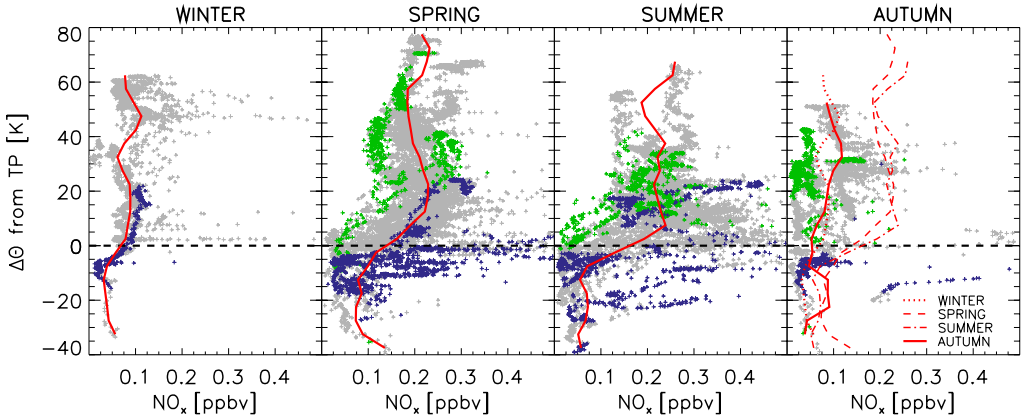

Fig. 8. Same as Fig. 6, but for NO_x(=NO+NO_2).

ACPD
5, 8649–8688, 2005

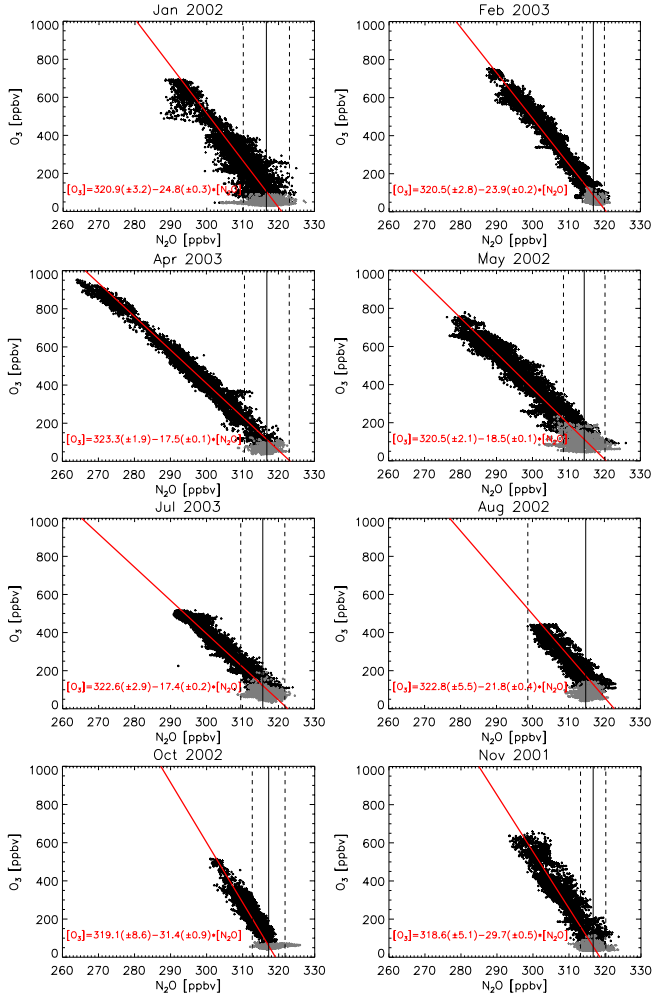

Fig. 9. Scatter plots between N_2O versus O_3 for each campaign. Red curves and formulae specify the measured correlations.

ACPD
5, 8649–8688, 2005

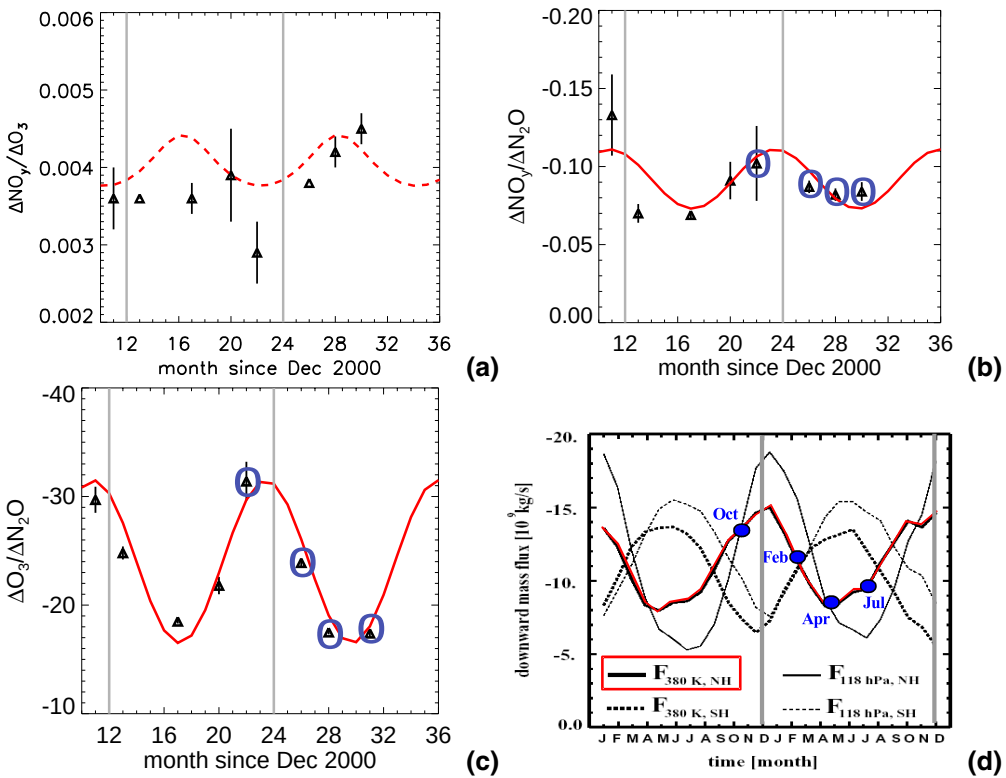

Fig. 10. Slopes of tracer-tracer correlations measured during the SPURT campaigns in the 'background' air of the LMS. **(a)** $\Delta NO_y/\Delta O_3$, **(b)** $\Delta NO_y/\Delta N_2O$, and **(c)** $\Delta O_3/\Delta N_2O$. The temporal evolution of the slopes exhibits a distinct seasonal cycle (given by the red lines) except for $\Delta NO_y/\Delta O_3$ (indicated by the red dashed line). **(d)** Downward mass fluxes through different reference surfaces adapted from Appenzeller et al. (1996). Reproduced by permission of American Geophysical Union. Here, the red line indicates the mass flux across the 380 K potential temperature surface being in phase with the seasonal cycle of the observed correlation slopes. Blue circles mark the months during which the SPURT campaigns were conducted.

ACPD
5, 8649–8688, 2005

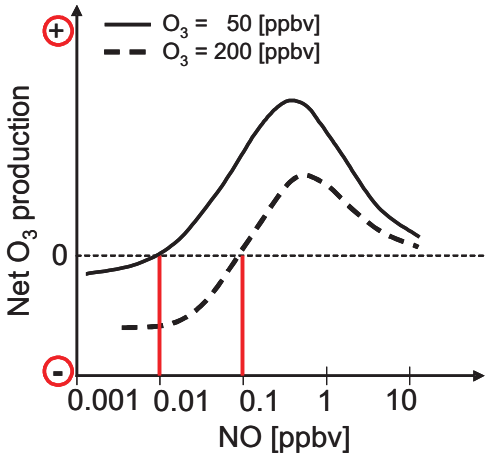

Fig. 11. Theoretical scheme of the net O_3 production (thick black lines) and critical NO values (marked by the red lines) depending on the background O_3 mixing ratios as derived from chemical box model calculations of Grooss et al. (1998). Thin black dashed line indicates zero O_3 production.

ACPD
5, 8649–8688, 2005

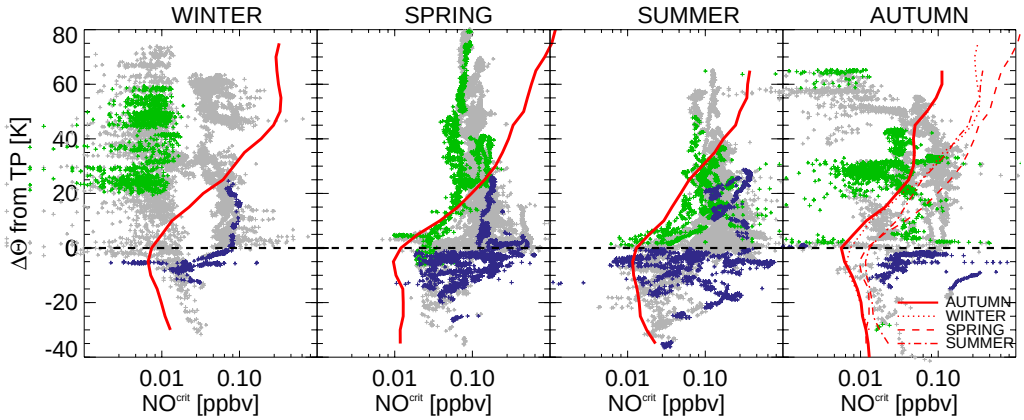

Fig. 12. Vertical profiles of critical NO values as a function of ΔΘ from the tropopause (defined by 2 PVU) and for different seasons (red lines). Blue crosses denote measurements with ϕ_e south from 35° N, light grey crosses with ϕ_e between 35° N and 65° N, and green crosses with ϕ_e north from 65° N. To allow direct comparison, the winter, spring and summer profiles are plotted in the autumn graph again.

ACPD
5, 8649–8688, 2005